

# Advection fields in maps: II. Dynamo action in the stretch–fold–shear map

Andrew D. Gilbert

*Department of Mathematical Sciences, University of Exeter, EX4 4QE, U.K.*

---

## Abstract

The growth of magnetic field is considered in the stretch–fold–shear map in the limit of weak diffusion. Numerical results are given for insulating, perfectly conducting and periodic boundary conditions. The resulting eigenvalue branches and magnetic fields are related to eigenvalue branches for perfect dynamo action, obtained for zero diffusion using a complex variable formulation.

The effect of diffusion on these perfect dynamo modes depends on their structure, growth rate and the diffusive boundary conditions employed. In some cases, the effect of diffusion is a small perturbation, giving a correction going to zero in the limit of weak diffusion, with a scaling exponent given analytically. In other cases weak diffusion can entirely destroy a perfect dynamo branch. Diffusive boundary layers can also generate entirely new branches.

These different cases are elucidated, and within the framework of the asymptotic approximations used (which do not constitute a rigorous proof), it is seen that for all three boundary conditions employed, the stretch–fold–shear map is a fast dynamo.

*Key words:* Magnetic field, dynamo, fast dynamo, hyperbolic map, mixing, baker’s map.

---

## 1 Introduction

This paper concerns fast dynamo action in the stretch–fold–shear (SFS) map, an idealised dynamo model, introduced by Bayly & Childress (1988, 1989) to model the amplification of magnetic fields in chaotic flows. The model was inspired by numerical studies of flows of the form  $\mathbf{u} = (u_x, u_y, u_z)(x, y, t)$ , that is with two-dimensional dependence on spatial coordinates, but having all three components of flow. Examples of such flows were considered in Bayly & Childress (1988), Galloway & Proctor (1992), Klapper (1992) and Otani (1993), using either a continuous flow field or by means of ‘pulsing’ the flow and diffusion, that is, applying the flow (or corresponding Lagrangian mapping) and

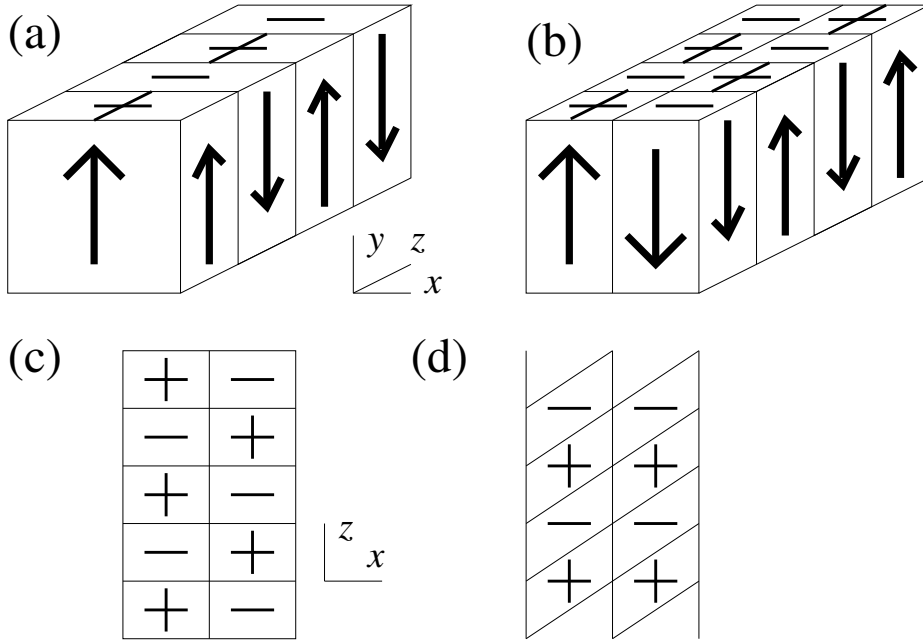


Fig. 1. The stretch–fold–shear map. (a) Magnetic field depending on  $z$  is stretched and folded with a baker’s map in the  $(x, y)$ -plane to give (b). In (c) the field orientation is shown in the  $(x, z)$ -plane, which after the shear operation gives (d). The effect of the stretch–fold–shear operations from (a) to (d) is to double the magnitude of field vectors and partially bring like-signed field together.

then allowing the magnetic field to diffuse. This technique was first exploited by Backus (1958) in proving the possibility of dynamo action in fluid flows.

An example of a flow used is that of Otani (1993),

$$\mathbf{u}(x, y, t) = 2 \cos^2 t (0, \sin x, \cos x) + 2 \sin^2 t (\sin y, 0, -\cos y), \quad (1.1)$$

and consists of two modulated helical waves. This produces amplification of magnetic fields, found by solving the induction equation,

$$\partial_t \mathbf{B} = \nabla \times (\mathbf{u} \times \mathbf{B}) + \varepsilon \nabla^2 \mathbf{B}, \quad (1.2)$$

numerically, taking  $\mathbf{B} \propto e^{ikz}$ . Here  $\varepsilon$  is a diffusivity or an inverse magnetic Reynolds number. Numerically a robust amplification of field is obtained with real growth rate tending to  $\gamma_0 \simeq 0.39$  for  $k \simeq 0.8$  as  $\varepsilon \rightarrow 0$ . The corresponding magnetic eigenfunctions, which take a Floquet form, however become more and more complicated in this limit.

The mechanism of magnetic field amplification is stretching and folding of sheets of field in the  $(x, y)$ -plane, followed by shearing in  $z$  which, through the  $e^{ikz}$  phase factor, allows like-signed belts of field to be brought together. This ‘stretch–fold–shear’ mechanism was identified by Bayly & Childress (1988), who then idealised it in the stretch–fold–shear map, depicted in figure 1. In

the model a magnetic field of the form

$$\mathbf{B}(x) = e^{ikz}b(x)\hat{\mathbf{y}} + \text{complex conjugate} \quad (1.3)$$

reduces to a single one-dimensional complex function  $b(x)$ . We take this to be defined on the interval  $[-1, 1]$  and to possess finite energy, with  $b$  lying in  $L^2[-1, 1]$ . The dynamo process depicted in figure 1 corresponds to the action of a linear operator  $T$  on  $b$ , defined below in (2.1). The mathematical problem is to understand the evolution of magnetic fields under repeated applications of  $T$  and some form of diffusion  $H_\varepsilon$ , in the limit of weak diffusion (see below for precise definitions). The main issue is to show that growth of fields under repeated iteration of the combined operator  $T_\varepsilon \equiv H_\varepsilon T$  is robust in this limit of weak diffusion,  $\varepsilon \rightarrow 0$ , and despite the magnetic eigenfunctions becoming more and more fine-scaled. Because of this fine scaling, it is unclear whether any meaning at all can be assigned to eigenfunctions with strictly zero diffusion,  $\varepsilon = 0$ .

A key advance by Bayly & Childress (1989) was to realise that the adjoint operator  $T_\varepsilon^*$  (working in the space of  $L^2$  functions) apparently possesses smooth eigenfunctions in the limit of small  $\varepsilon$ , and this can be exploited to study the limit  $\varepsilon \rightarrow 0$  numerically. In fact one can set  $\varepsilon = 0$  and use  $T^*$  to obtain certain smooth eigenfunctions numerically, even though the corresponding computations for  $T$  are essentially meaningless! This suggested the possible approach of studying  $T^*$ , taking the smooth eigenfunctions generated, and then introducing diffusion as a perturbation. This is not straightforward since diffusion is not always a small perturbation for baker's maps: the discontinuity in the mapping can lead to diffusive boundary layers, as we shall find (see also Childress & Gilbert, 1995, §9.6.2).

The aim of the present series of papers is to introduce analytical tools to justify the above approach of studying  $T^*$  for zero diffusion, and to discuss the limit of weak diffusion. Our work builds on studies of Rugh (1992) and Mestel, Osbaldestin & Winn (2000), and is closely linked to computations of fast dynamo growth rates using periodic orbit sums (Aurell & Gilbert, 1993; Balmforth *et al.*, 1993).

In paper I (Gilbert, 2002), the adjoint SFS dynamo operator  $T^*$  was discussed using a complex variable formulation. The idea was to consider adjoint eigenfunctions,  $T^*c = \lambda c$ , but to restrict consideration from functions  $c(x)$  defined on  $[-1, 1]$  and lying in  $L^2[-1, 1]$ , to a subset  $\mathcal{B}^*$  of functions  $c(z)$  that are analytic in a complex disc containing the real line segment  $[-1, 1]$ . This leads to a new<sup>1</sup> operator  $\mathcal{T}^*$  on this restricted space which has well-defined eigen-

---

<sup>1</sup> This operator was denoted  $S$  in paper I and the space  $\mathcal{B}^*$  was called  $\mathcal{B}$ . There are a number of other minor changes, our aim being to make the notation more intuitive for the purposes of this paper.

functions and eigenvalues; they are also eigenfunctions of the original adjoint operator  $T^*$  but have good smoothness properties. Furthermore taking the adjoint  $\mathcal{T}$  of  $\mathcal{T}^*$  gives an operator which is essentially the same as the original direct operator  $T$ , but acts in a larger space  $\mathcal{B}$  which includes distributions. It now becomes sensible to talk about direct eigenfunctions, not lying in  $L^2$  but in this bigger space; see Childress & Gilbert (1995), §9.5.2, Bayly (1992, 1994) and Rado (1993).

The focus of paper I was to prove ‘perfect dynamo action’, that is to take zero diffusion, and to show that  $\mathcal{T}^*$  has a growing eigenfunction, a ‘perfect mode’, corresponding to an eigenvalue  $\lambda$  with  $|\lambda| > 1$ . This was done by a mixture of analytical techniques involving ideas from the theory of pseudo-spectra (Trefethen, 1997), together with numerical computations. The result was that there are eigenvalues with  $|\lambda| > 1$  obtained when the operator  $\mathcal{T}^*$  is truncated to become a matrix of size  $N^2$ . The errors caused by this truncation could be bounded and are sufficiently small to guarantee that  $|\lambda|$  remains bounded above unity for the untruncated operator  $\mathcal{T}^*$ . Paper I involved no diffusion,  $\varepsilon = 0$ , and amounted to showing that the SFS dynamo amplifies magnetic fluxes in the absence of diffusion; this property of constructive folding of field appears to be the key property a chaotic flow must have to be a fast dynamo. This was stressed by Finn & Ott (1988) and Bayly & Childress (1989), but there are no general mathematical results, even applying to models as basic as the SFS map.

The aim of the present paper, paper II, is to reintroduce diffusion. The basic idea is that having identified smooth eigenfunctions of  $\mathcal{T}^*$  with no diffusion through the complex variable formulation in paper I, the effects of diffusion may be a small perturbation. This is what lay behind the original thinking of Bayly & Childress (1989) and is generally supported by their numerical studies. We begin in section 2 by studying numerically the limiting behaviour of eigenvalues for weak diffusion and different boundary conditions. This leads straightforwardly to suggest possible criteria for a given perfect mode of  $\mathcal{T}^*$  to be ‘robust’ to diffusion, that is, to correspond to a limiting eigenmode of  $T_\varepsilon^*$  as  $\varepsilon \rightarrow 0$ . These criteria depend on the boundary conditions, and sensitivity to boundary conditions in such dynamo problems has been noted by Bayly & Childress (1988) and Finn & Ott (1990).

To put some theory behind these numerical results, in section 3 we summarise what is known about perfect dynamo modes, extending the results from paper I. We compare eigenfunctions of  $T_\varepsilon^*$ , with diffusion  $\varepsilon > 0$ , and those of  $\mathcal{T}^*$ , without diffusion. In some cases these correspond, but the eigenfunctions of  $\mathcal{T}^*$  need to be supplemented by a thin boundary layer, whose scale goes to zero as  $\varepsilon \rightarrow 0$ . In sections 4 and 5, we study the effects of diffusion and obtain scaling laws for the diffusive corrections, as well as criteria for when diffusion will or will not destroy a branch of perfect dynamo modes. Few explicit calculations

are possible, but in section 6 we calculate the diffusive corrections for a branch of perfect modes, by solving a boundary layer integral equation numerically. We offer concluding discussion in section 7.

The aim has been to make this paper essentially self-contained, reproducing the few key results needed from paper I. The style is however different from paper I. Whereas in paper I we bounded errors on eigenvalues rigorously (with the aid of numerical computations), we now adopt more of a perturbation approach, using some asymptotic matching of solutions. This is not rigorous in the sense of being able to bound the errors using functional analytic techniques; however it allows us to isolate the key features of diffusion in these systems. A third paper, III (Gilbert, 2004), again self-contained and complementary, discusses related problems involving the decay of passive scalar scalars in baker's maps with uneven stretching.

## 2 Numerical results with diffusion

We pick up the basic definitions from paper I, which may be consulted for more background. The SFS dynamo process is depicted schematically in figure 1; the corresponding SFS dynamo operator is given by

$$Tb(x) = \begin{cases} 2e^{-i\alpha kx}b(1+2x) & (-1 \leq x \leq 0), \\ -2e^{-i\alpha kx}b(1-2x) & (0 < x \leq 1), \end{cases} \quad (2.1)$$

and acts on complex magnetic fields  $b(x)$  defined for  $-1 \leq x \leq 1$ . The corresponding actual magnetic field is given in (1.3). An alternative way of expressing  $T$  is to take  $b(x)$  to be defined for all real  $x$ , but to be zero outside the interval  $[-1, 1]$ . In this case we may write

$$Tb(x) = 2e^{-i\alpha kx}b(1+2x) - 2e^{-i\alpha kx}b(1-2x). \quad (2.2)$$

In either case we see that the parameters  $\alpha$  and  $k$  occur in the combination  $\alpha k$  and so it is convenient to set  $k = 1$  from here on, with little loss of generality.

The key effects of the operator  $T$  are the reduction in field scale by a factor two, together with stretching and folding. There are also the complex phase shifts induced by shear in the  $z$ -direction given by a shear parameter  $\alpha \geq 0$ , which are essential to the operation of the dynamo. Note that the baker's map is 'even', that is the stretching of field and the compression of structure in  $x$  is the same, by a factors of 2, in the two pieces. Uneven stretching (as in paper III) could be introduced, but would simply add an extra parameter to the dynamo problem.

In this paper we incorporate pulsed diffusion: we apply the SFS map instantaneously, and then allowing the field to diffuse for a time unity with diffusivity  $\varepsilon$ . We apply  $\partial_t b = \varepsilon \partial_x^2 b$  to the magnetic field, with one of the following three boundary conditions applied at the end points  $x = \pm 1$ ,

$$b(1) = b(-1) = 0, \quad (\text{I}), \quad (2.3)$$

$$\partial_x b(1) = \partial_x b(-1) = 0, \quad (\text{C}), \quad (2.4)$$

$$b(x) \text{ periodic}, \quad (\text{P}), \quad (2.5)$$

that is, insulating (I), perfectly conducting (C) and periodic (P). In each case this can be achieved by integrating the magnetic field against a heat kernel  $H_\varepsilon(x, y)$  incorporating boundary conditions. We use the same symbol  $H_\varepsilon$  for each of the resulting (self-adjoint) operators on the magnetic field,

$$H_\varepsilon b(x) \equiv H_\varepsilon^* b(x) = \int_{-1}^1 H_\varepsilon(x, y) b(y) dy. \quad (2.6)$$

We have for insulating (upper sign) and conducting (lower sign),

$$H_\varepsilon(x, y) = \sum_{p \text{ even}} G_\varepsilon(x - y - 2p) \mp \sum_{p \text{ odd}} G_\varepsilon(x + y - 2p), \quad (\text{I/C}), \quad (2.7)$$

and for the periodic boundary condition

$$H_\varepsilon(x, y) = \sum_p G_\varepsilon(x - y - 2p), \quad (\text{P}). \quad (2.8)$$

In each case  $p$  ranges over the integers, and

$$G_\varepsilon(x) = \varepsilon^{-1/2} g(x/\sqrt{\varepsilon}), \quad (2.9)$$

with

$$g(x) = (4\pi)^{-1/2} \exp(-x^2/4). \quad (2.10)$$

Note that we neglect the effect of diffusion on the variation of the true magnetic field (1.3) in the  $z$ -direction. Reintroducing  $k$ , this would simply incorporate an extra factor  $e^{-\varepsilon k^2}$ , that is, a large- $k$  cut-off. We return to this point in the final discussion section.

We may now define the dynamo operator

$$T_\varepsilon = H_\varepsilon T. \quad (2.11)$$

Our focus is on eigenvalues and eigenfunctions

$$T_\varepsilon b = \lambda b, \quad (2.12)$$

particularly when there is dynamo action,  $|\lambda| > 1$ , in the limit of small  $\varepsilon$ .

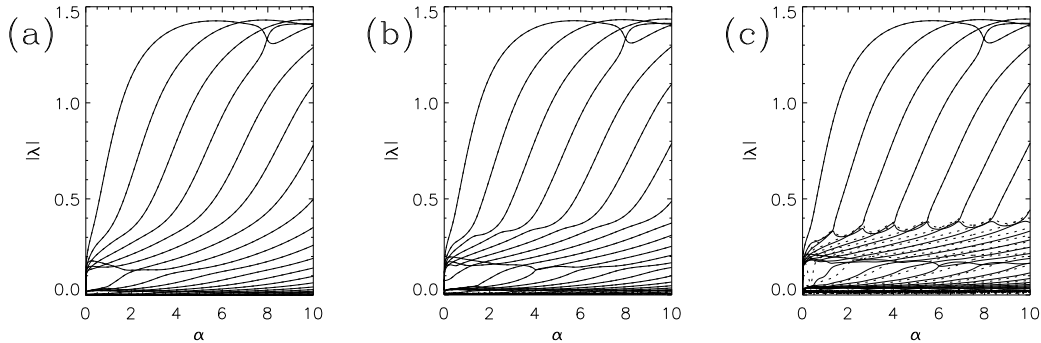


Fig. 2. Moduli of eigenvalues  $|\lambda|$  as a function of  $\alpha$  for the insulating boundary condition (I). The values for the diffusivity and resolution are (a)  $\varepsilon = 10^{-4}$ ,  $N = 512$ , (b)  $\varepsilon = 10^{-5}$ ,  $N = 1024$  and (c)  $\varepsilon = 10^{-6}$ ,  $N = 1024$ .

The above forms (2.7) and (2.8) for the diffusion kernel  $H_\varepsilon$  will be useful when we develop boundary layer theory later on. However from the point of view of obtaining numerical results for growth rates as a function of  $\varepsilon$  and, having in mind magnetic fields that have finite energy, it is better to use orthonormal bases for  $L^2[-1, 1]$  which satisfy the boundary conditions automatically. We therefore define an  $L^2$  inner product by

$$(b, c) = \int_{-1}^1 b(x)c(x) dx, \quad (2.13)$$

and the  $L^2$  norm is given by

$$\|b\|^2 = (\bar{b}, b), \quad (\bar{b}(x) \equiv \overline{b(x)}). \quad (2.14)$$

The absence of complex conjugation in the definition (2.13) is designed to avoid confusion when we replace  $x$  by a complex variable in the next section. (It also yields a number of inessential differences between this paper and paper I, which we will not flag in detail.) For similar reasons, to obtain results numerically it is convenient to use a real orthonormal basis  $\{\psi_n(x)\}$  satisfying

$$(\psi_m, \psi_n) = \delta_{mn}. \quad (2.15)$$

Representing a magnetic field by the set of complex coefficients  $\{b_n\}$  given by

$$b(x) = \sum_n b_n \psi_n(x), \quad b_n = (\psi_n, b), \quad (2.16)$$

we may compute the action of  $T$  or  $H_\varepsilon$  using the matrix elements

$$T_{mn} = (\psi_m, T\psi_n), \quad H_{\varepsilon mn} = (\psi_m, H_\varepsilon \psi_n). \quad (2.17)$$

The bases used for the (I), (C) and (P) boundary conditions, and the corresponding matrix elements, are listed in appendix A.

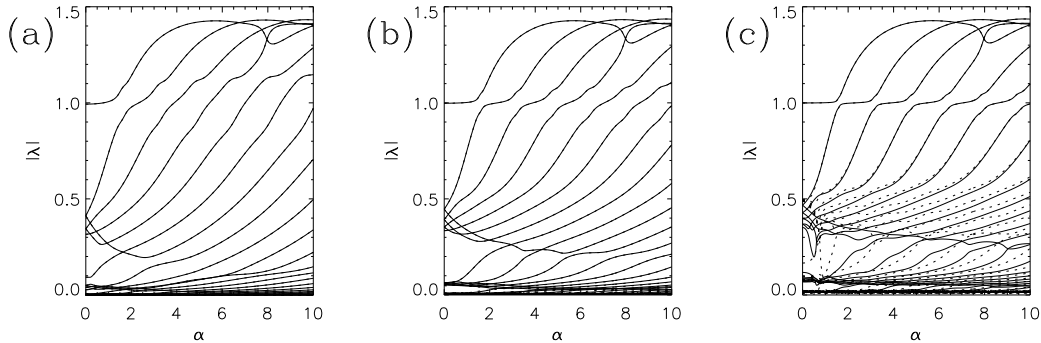


Fig. 3. Moduli of eigenvalues  $|\lambda|$  as a function of  $\alpha$  for the conducting boundary condition (C), as in figure 2.

We obtain numerical results by truncating the matrices in (2.17) to a size  $N^2$  and applying a numerical eigenvalue solver from the NAG library. Results for eigenvalues with the insulating (I) boundary condition are shown in figure 2 with  $|\lambda|$  shown as a function of the shear parameter  $\alpha$  (using a resolution 0.01 in  $\alpha$ ). In (a,b,c) the diffusivity  $\varepsilon$  is decreased, the resolution  $N$  being increased appropriately. Also, to give an indication of accuracy, similar results at a resolution  $N/2$  are overplotted with dotted lines in all three subfigures, but this is only visible in figure 2(c). This is also done in figures 3, 4, 9, 11 below.

We observe that for the insulating boundary condition the eigenvalue branches appear to converge cleanly for

$$|\lambda| > 1/4, \quad (\text{I}). \quad (2.18)$$

This includes all the growing, dynamo modes, that is those with  $|\lambda| > 1$  and so gives clear numerical evidence for fast dynamo action with this boundary condition. For  $|\lambda| < 1/4$  there is no clear picture yet emerging for  $\varepsilon \rightarrow 0$ .

Note that at  $\alpha = 0$ , when there is no shear, all the branches go down to  $\lambda = 0$ . This is a consequence of the fact that the action of  $T_\varepsilon$  on the appropriate basis (A.1) is a doubling of wavenumber and a diffusive damping:

$$T_\varepsilon \sin \frac{1}{2}n\pi(x+1) = 2e^{-\varepsilon n^2\pi^2} \sin \frac{1}{2}2n\pi(x+1) \quad (2.19)$$

(see also Childress & Gilbert (1995), §9.5.3). As is easily checked by substituting into (2.12), this implies that at  $\alpha = 0$  there are no eigenfunctions and that magnetic fields undergo superexponential decay. This feature was also observed by Finn & Ott (1990), who noted that this rapid decay appeared to be special for the insulating boundary condition and even stretching in the underlying baker's map. Note that this case of  $\alpha = 0$  is closely related to the behaviour of passive scalars in the baker's map; see paper I, §4.3, and paper III.

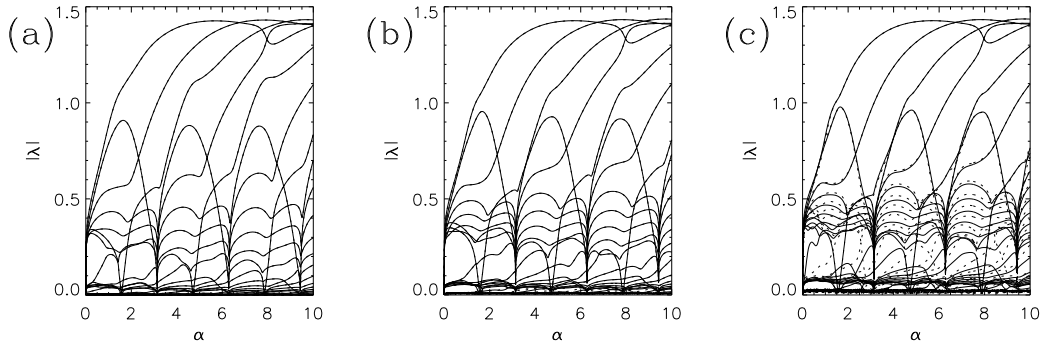


Fig. 4. Moduli of eigenvalues  $|\lambda|$  as a function of  $\alpha$  for the periodic boundary condition (P), as in figure 2.

Results for the conducting (C) boundary condition are shown in figure 3. Here, now for

$$|\lambda| > 1/2, \quad (\text{C}), \quad (2.20)$$

we appear to have convergence to the same branches as in figure 2, except that there is an additional branch emerging with  $|\lambda| = 1$ : this will be referred to below as the ‘exact branch’. For growing, dynamo modes, having  $|\lambda| > 1$  the picture emerging is the same as for the insulating boundary condition.

Note that for  $\alpha = 0$ , instead of superexponential decay for (C), we now have an eigenvalue branch with  $|\lambda| \rightarrow 1$  as  $\varepsilon \rightarrow 0$ . This indicates the sensitivity to boundary conditions that can occur. In fact the behaviour of the growth rate is

$$\lambda \simeq 1 - 2K\sqrt{\varepsilon}, \quad K \simeq 0.33 \quad (\alpha = 0, \varepsilon \rightarrow 0), \quad (2.21)$$

and we shall later, in section 6, track down the origin of this scaling and the constant  $K$ .

Finally figure 4 shows results for the periodic boundary condition. For

$$|\lambda| > 1/2, \quad (\text{P}), \quad (2.22)$$

we appear to have convergence to the branches seen for insulating and the conducting boundary condition. However the exact branch with  $|\lambda| = 1$  seen in figure 3 is absent, and we appear to have an additional branch with three peaks at  $|\lambda| \simeq 1$  within the range of  $\alpha$  surveyed. At  $\alpha = 0$  we have no eigenfunctions and superexponential decay of field for the (P) boundary condition, using a similar argument to that employed above for the case (I).

Our aim in what follows is to understand the features of these three sets of results. For  $|\lambda| > 1$  all three sets of results agree nicely, and point the way to fast dynamo action, with limiting growth rates as  $\varepsilon \rightarrow 0$  that are independent of boundary conditions. We will track down how the growth rates tend to these limiting values. We will also understand why the exact branch is present in

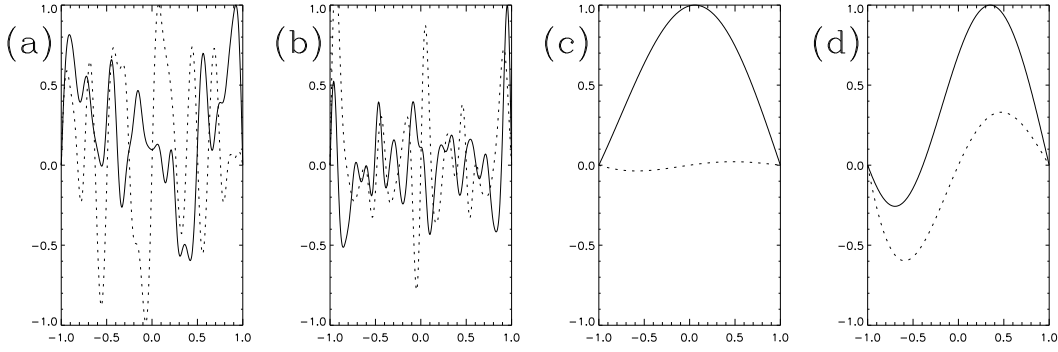


Fig. 5. Eigenfunctions for  $\alpha = 2$ ,  $\varepsilon = 10^{-3}$  and insulating (I) boundary condition, showing real part (solid) and imaginary part (dotted). (a) depicts the most unstable and (b) the next most unstable eigenmode of  $T_\varepsilon$ . (c) and (d) show the corresponding eigenmodes of  $T_\varepsilon^*$ .

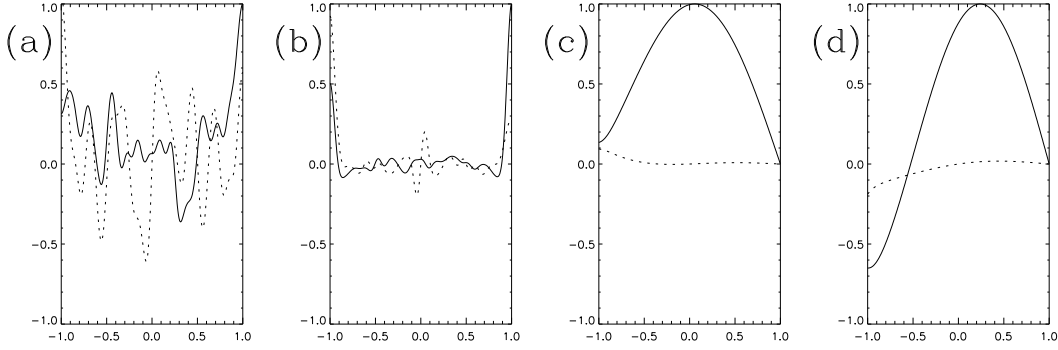


Fig. 6. Eigenfunctions as in figure 5 but for the conducting (C) boundary condition.

figure 3 and not elsewhere, justify the (rather precisely stated) results (2.18), (2.20) and (2.22), and discover the origin of the additional branch in figure 4.

We now plot the corresponding eigenfunctions for the case  $\alpha = 2$  and  $\varepsilon = 10^{-3}$ , for each boundary condition. Here for each eigenvalue  $\lambda$  we may reconstruct the direct eigenfunction  $b(x)$  of (2.12) using the right eigenvector of the truncated matrix  $T_{\varepsilon mn}$ , or alternatively compute the adjoint eigenfunction  $c(x)$  from the left eigenvector. An adjoint eigenfunction satisfies

$$T_\varepsilon^* c = \lambda c, \quad (2.23)$$

where  $T_\varepsilon^*$  is the adjoint operator, defined by  $(c, T_\varepsilon b) = (T_\varepsilon^* c, b)$  with the inner product (2.13), explicitly,

$$T_\varepsilon^* = T^* H_\varepsilon^* \quad (H_\varepsilon \equiv H_\varepsilon^*), \quad (2.24)$$

with

$$T^* c(x) = e^{-i\alpha\frac{1}{2}(x-1)} c\left(\frac{1}{2}(x-1)\right) - e^{-i\alpha\frac{1}{2}(1-x)} c\left(\frac{1}{2}(1-x)\right). \quad (2.25)$$

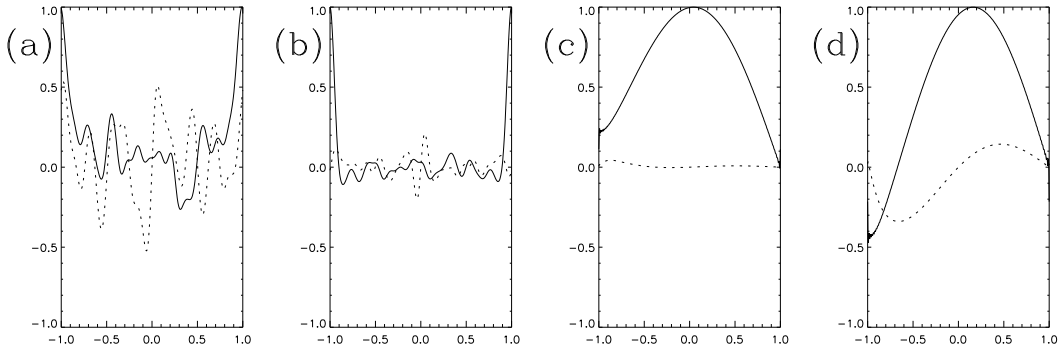


Fig. 7. Eigenfunctions as in figure 5 but for the periodic (P) boundary condition.

For the insulating boundary condition, figure 5 shows the leading direct eigenfunctions  $b(x)$  of  $T_\varepsilon$  in (a,b), and the leading adjoint eigenfunctions  $c(x)$  of  $T_\varepsilon^*$  in (c,d). The key point to note is that whereas the direct eigenfunctions are quite rough (and indeed gain finer and finer structure as  $\varepsilon$  is decreased), the adjoint eigenfunctions are really quite smooth, because the effect of the operator  $T^*$  in (2.25) is to stretch out and average fine structure (Bayly & Childress, 1989). In fact the adjoint eigenfunctions have a structure of a ‘mainstream’ part, in which diffusion is insignificant, with a diffusively controlled boundary layer at the left end,  $x = -1$ , as we shall see. By contrast, the folding in the baker’s map means that the direct eigenfunctions have boundary layers in the interior, and more of these emerge as  $\varepsilon$  is reduced. Figures 6 and 7 show the corresponding eigenfunctions for the two most unstable branches with (C) and (P) boundary conditions respectively. Again the key feature is that the adjoint eigenfunctions are well-behaved, in contrast to the direct eigenfunctions.

Another point to note is that the first adjoint eigenfunction in each figure, that is in 5(c), 6(c) and 7(c), corresponds to the same eigenvalue branch for  $\lambda$  (see figures 2, 3 and 4). These adjoint eigenfunctions indeed have a very similar structure, only differing close to  $x = -1$ . In fact the relatively large value of  $\varepsilon$  used is chosen so that the differences can be seen, as they shrink away if  $\varepsilon$  is much further reduced. By contrast the second adjoint eigenfunctions depicted in 5(d), 6(d) and 7(d) all correspond to different eigenvalue branches for  $\lambda$ .

### 3 Eigenvalues and eigenfunctions without diffusion

We now consider what happens if diffusion is turned off. Our aim is to summarise the key points we shall need from paper I in a non-technical way (skating over some detail); see Kato (1980), Bollobás (1990) and Childress & Gilbert (1995) for background. The situation is summarised in figure 8.

First consider the operators  $T_\varepsilon$  and  $T_\varepsilon^*$  for non-zero diffusion  $\varepsilon > 0$ ; these are

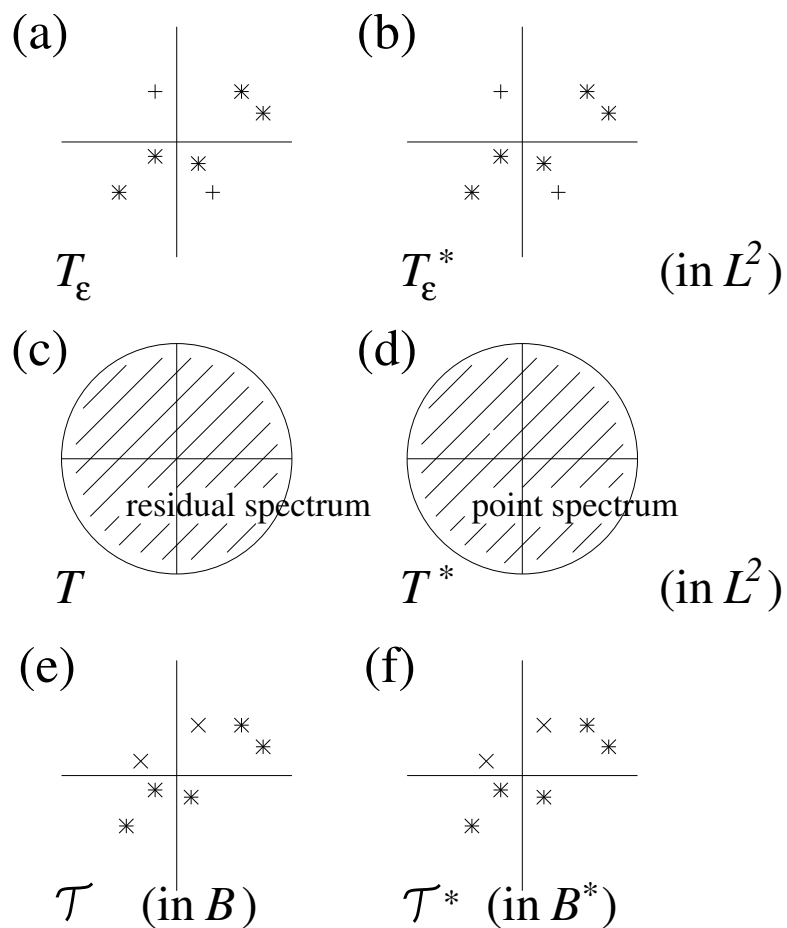


Fig. 8. Schematic figure showing spectra of operators and their adjoints in the complex plane. Spectra of (a)  $T_\varepsilon$  and (b)  $T_\varepsilon^*$  for  $\varepsilon \ll 1$ . Spectra of (c)  $T$  and (d)  $T^*$ . Spectra of (e)  $\mathcal{T}$  and (f)  $\mathcal{T}^*$ .

compact operators in  $L^2$  because of the effect of diffusion, however weak, in suppressing small scales. They therefore have only point spectrum, eigenvalues, with corresponding direct and adjoint eigenfunctions. Direct eigenfunctions, that is of  $T_\varepsilon$ , gain finer and finer structure as  $\varepsilon \rightarrow 0$ , while those of  $T_\varepsilon^*$  appear smooth and well-behaved (except for possible boundary layers at the left-hand side). The eigenvalues are depicted schematically in figure 8(a,b) (shown by + or \*).

Now suppose diffusion is turned off. Then  $T_0 \equiv T$  has no eigenfunctions at all in  $L^2$ , unsurprisingly. Perhaps more surprisingly  $T_0^* \equiv T^*$  has a whole disc  $|\lambda| < 2$  of eigenvalues, but the corresponding eigenfunctions are generally not infinitely differentiable. The situation is depicted in figure 8(c,d), and leaves us in a poor situation to study the limit of weak diffusion.

The key idea in paper I was to consider  $T^*$  with zero diffusion, but to fix a constant  $r > 1$  and restrict our attention to functions  $c$  in the space  $\mathcal{B}^*$  of complex functions analytic in the open disc  $\mathcal{D}$ ,  $|z| < r$ , and continuous in the

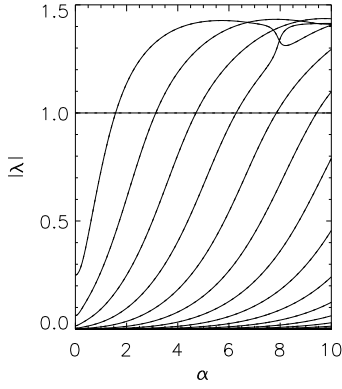


Fig. 9. Eigenvalues  $|\lambda|$  of  $\mathcal{T}^*$  or  $\mathcal{T}$  as a function of  $\alpha$ , with  $N = 128$ .

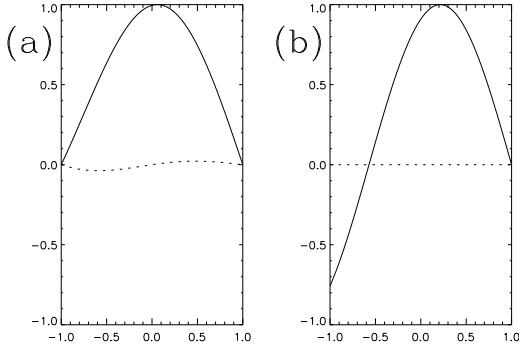


Fig. 10. Eigenfunctions for  $\alpha = 2$  (and no diffusion); (a) depicts the most unstable and (b) the next most unstable eigenmode of  $\mathcal{T}^*$  in  $\mathcal{B}^*$ .

closed disc  $\bar{\mathcal{D}}$ , with a supremum norm,

$$\|c\| = \sup_{z \in \bar{\mathcal{D}}} |c(z)|. \quad (3.1)$$

This new space  $\mathcal{B}^*$  is a subspace of  $L^2$ , but functions in it have much nicer properties, for example being infinitely differentiable. Also, the restriction of  $\mathcal{T}^*$  to  $\mathcal{B}^*$ , which we denote  $\mathcal{T}^*$ , is given again by the formula (2.25), and is a compact operator. The reason for this is that  $\mathcal{T}^*$  is ‘analyticity improving’: if a function  $c(z)$  is analytic in  $\mathcal{D}$ , then  $\mathcal{T}^*c$  is analytic in the larger disc  $|z| < 2r - 1$ . Iterating this process, we see that eigenfunctions of  $\mathcal{T}^*$  with non-zero eigenvalue  $\lambda$  are in fact entire, analytic in all of  $\mathbb{C}$ . Using (3.1) one can also show that eigenfunctions grow no faster than exponentially in the complex plane. The property of compactness means that  $\mathcal{T}^*$  and its adjoint  $\mathcal{T}$  have a spectrum of only point eigenvalues, as shown in figure 8(e,f) by  $\times$  or  $*$ . These were obtained numerically in paper I and are shown as a function of  $\alpha$  in figure 9; the corresponding leading eigenfunctions are shown for  $\alpha = 2$  in figure 10. They may also be obtained by methods based on periodic orbit sums (Rugh, 1992; Aurell & Gilbert, 1993; Balmforth *et al.*, 1993).

Unfortunately for the stretch–fold–shear model very few of the corresponding

eigenfunctions are known explicitly (contrast the case of passive scalars in paper III). However for zero shear,  $\alpha = 0$ , we have eigenfunctions

$$c_0(z) = z - 1, \quad \lambda = 1, \quad (3.2a)$$

$$c_1(z) = z^3 - 3z^2 - z + 3, \quad \lambda = \frac{1}{4}, \quad (3.2b)$$

$$c_2(z) = z^5 - 5z^4 - \frac{10}{3}z^3 + 30z^2 + \frac{7}{3}z - 25, \quad \lambda = \frac{1}{16}, \quad (3.2c)$$

and for any shear we have what we shall describe as the ‘exact branch’,

$$c_0(z) = e^{i\alpha(z-1)} - e^{i\alpha(1-z)} = 2i \sin \alpha(z-1), \quad \lambda = e^{i\alpha} \quad (3.3)$$

(Dr. B.J. Bayly, personal communication, and Rado (1993)). This is the horizontal branch in figure 9; see also figure 10(b). Note that (3.2a) and (3.3) coincide at  $\alpha = 0$ , up to normalisation.

Useful properties of eigenfunctions can be obtained by evaluating  $\mathcal{T}^*c = \lambda c$  at  $z = \pm 1$  to give

$$c(1) = 0 \quad (\lambda \neq 0), \quad (3.4)$$

$$c(-1) = 0 \quad (\lambda \neq 0, e^{i\alpha}). \quad (3.5)$$

Thus, except for the exact branch (and the uninteresting case  $\lambda = 0$ ), every eigenfunction is zero at the two endpoints; this will become important in the boundary layer theory of section 5.

The strategy we will pursue is to attempt to link the eigenvalues of  $\mathcal{T}^*$  and  $\mathcal{T}$  in figure 8(e,f) for zero diffusion, to those of  $T_\varepsilon^*$  and  $T_\varepsilon$  for weak diffusion, encouraged by the obvious links between figure 9 for  $\varepsilon = 0$  and figures 2, 3 and 4 for  $\varepsilon \ll 1$  (as well as the corresponding eigenfunctions). Some terminology (similar to that in Childress & Gilbert (1995)) may be helpful :

- (i) A *perfect mode* is an eigenfunction pair of  $\mathcal{T}$  and  $\mathcal{T}^*$  with eigenvalue  $\lambda \neq 0$  (shown as  $\times$  or  $*$  in figure 8(e,f)).
- (ii) A perfect mode with eigenvalue  $\lambda$  is *robust* to diffusion if there is an eigenvalue  $\lambda_\varepsilon$  of  $T_\varepsilon$  and  $T_\varepsilon^*$  with  $\lambda_\varepsilon \rightarrow \lambda$  as  $\varepsilon \rightarrow 0$  ( $*$  in 8(e,f)). The corresponding limiting eigenfunction pair of  $T_\varepsilon$  and  $T_\varepsilon^*$  is called *non-diffusive* ( $*$  in 8(a,b)).
- (iii) A perfect mode which is not robust is called *delicate*; it completely disappears under the effects of diffusion, no matter how weak ( $\times$  in 8(e,f)).
- (iv) An eigenmode pair for  $T_\varepsilon$  and  $T_\varepsilon^*$  that fails to be non-diffusive is called *diffusive*; it owes its existence entirely to diffusion ( $+$  in 8(a,b)).

The robustness of a perfect mode depends on the boundary condition and on the structure of the mode itself. Our aim is to obtain the criteria for a perfect mode to be robust to diffusion, that is, (2.18), (2.20), (2.22) for all branches other than the exact branch. When such a mode is robust, we want to obtain

the leading correction that arises through the effects of diffusion. Also we will find out why the exact branch is robust only for the (C) boundary condition, and the origin of the diffusive branch (with three peaks) that appears for the (P) boundary condition in figure 4.

We have discussed the restricted operator  $\mathcal{T}^*$  acting on the space  $\mathcal{B}^* \subset L^2$  and we now consider its adjoint  $\mathcal{T}$  and the space  $\mathcal{B}$  in which it acts<sup>2</sup>; the key idea is that  $\mathcal{B}$  is ‘bigger’ than  $L^2$ , and so whereas  $T$  has no eigenfunctions in  $L^2$ , the operator  $\mathcal{T}$  has well-defined eigenfunctions which can be calculated numerically; these can be thought of as distributions. We again summarise paper I, skating over a few technical points.

Suppose we are given a function  $c \in \mathcal{B}^*$ ; the action of a member  $b$  of the adjoint space  $\mathcal{B}$  can be written as

$$\langle b, c \rangle = \frac{1}{2\pi i} \oint_{\partial\mathcal{D}} b(z)c(z)dz \quad (3.6)$$

and any  $b \in \mathcal{B}$  has the property that it is analytic in the region  $\mathbb{C} \setminus \bar{\mathcal{D}}$ . Also we can add an entire function to  $b$  without affecting the value of this integral, so we are really considering  $b$  as an equivalence class of functions that differ by an entire function (but we will not adopt a formal notation for this).

The adjoint operator to  $\mathcal{T}^*$  is

$$\mathcal{T}b(z) = 2e^{-iaz}[b(1+2z) + b(1-2z)]. \quad (3.7)$$

Bases of  $\mathcal{B}$  and  $\mathcal{B}^*$  are given by

$$e_n(z) = r^n z^{-n-1}, \quad e_n^*(z) = z^n r^{-n}, \quad \langle e_m, e_n^* \rangle = \delta_{mn} \quad (3.8)$$

and eigenfunctions of  $\mathcal{T}$  and  $\mathcal{T}^*$  may be expanded as

$$b(z) = \sum_{n=0}^{\infty} \beta_n z^{-n-1}, \quad c(z) = \sum_{n=0}^{\infty} \gamma_n z^n, \quad (3.9)$$

giving

$$\langle b, c \rangle = \sum_{n=0}^{\infty} \beta_n \gamma_n. \quad (3.10)$$

Matrix elements of  $\mathcal{T}^*$  with respect to these bases are given in appendix B. Truncating these matrices to  $N^2$  elements allows easy computation of eigenvalues (see figure 9), left eigenvectors  $\{\beta_n\}$  and right eigenvectors  $\{\gamma_n\}$  (see figure 10).

---

<sup>2</sup> Strictly these should be denoted  $\mathcal{T}^{**}$  and  $\mathcal{B}^{**}$ , but our aim is to keep the notation straightforward.

Just as for eigenfunctions of  $\mathcal{T}^*$ , few are known explicitly for  $\mathcal{T}$ . However corresponding to (3.2) we have

$$b_j(z) = (z-1)^{-2j-1} - (z+1)^{-2j-1}, \quad \lambda = 2^{-2j} \quad (\alpha = 0). \quad (3.11)$$

These satisfy  $\langle b_j, c_k \rangle = 2(2j+1)\delta_{jk}$ . Also note that for  $\alpha = 0$ ,

$$c_j'' = 2j(2j+1)c_{j-1}, \quad b_j'' = (2j+1)(2j+2)b_{j+1}, \quad (3.12)$$

since  $(\mathcal{T}^*c)'' = \frac{1}{4}\mathcal{T}^*c''$  and  $(\mathcal{T}b)'' = 4\mathcal{T}b''$ .

Corresponding to the exact branch (3.3) we have

$$b_0(z) = e^{-i\alpha}(z-1)^{-1} - e^{i\alpha}(z+1)^{-1}, \quad \lambda = e^{i\alpha}, \quad (3.13)$$

for any  $\alpha$ , with

$$\langle b_0, c_0 \rangle = 2ie^{i\alpha} \sin 2\alpha. \quad (3.14)$$

There is a degeneracy that occurs when  $\alpha = n\pi/2$ , corresponding to mode crossings (in the complex plane) between the exact branch and other branches (see figure 9). Note for (3.13) that  $\mathcal{T}b_0 - \lambda b_0$  does not immediately appear to be zero, but as it is an entire function

$$(\mathcal{T}b_0 - \lambda b_0)(z) = \lambda[(e^{-i\alpha z} - e^{-i\alpha})(z-1)^{-1} - (e^{-i\alpha z} - e^{i\alpha})(z+1)^{-1}] \quad (3.15)$$

once removable singularities at  $z = \pm 1$  are taken into account, it is equivalent to zero, given our remarks about equivalence classes above.

Finally we need to link  $\mathcal{T}$  to the original  $T$ ; certainly (2.2) and (3.7) are the same up to a sign! It turns out (see paper I) that eigenfunctions of  $\mathcal{T}$  are in fact analytic in  $\mathbb{C}$  except on the real line segment  $[-1, 1]$ . Given that they are equivalence classes modulo addition of entire functions, this means they are termed ‘hyperfunctions’ supported on  $[-1, 1]$  as discussed in Schlichtkrull (1984). Suppose we have a magnetic field  $b(x)$  defined on  $[-1, 1]$ , as at the start of this paper. We can define a corresponding hyperfunction  $\mathcal{F}b$  via

$$\mathcal{F}b(z) = \int_{-1}^1 \frac{b(x)}{z-x} dx, \quad (3.16)$$

so that the field distribution in  $b$  is encoded into the singularities of  $\mathcal{F}b$  along  $[-1, 1] \subset \mathbb{C}$ . With this definition the actions of  $\mathcal{T}$  and  $T$  correspond; we have for  $b \in L^2$ , and  $c \in \mathcal{B}^* \subset L^2$

$$\mathcal{T}\mathcal{F}b = \mathcal{F}Tb, \quad \langle \mathcal{F}b, c \rangle = (b, c). \quad (3.17)$$

We can then interpret the eigenfunctions given explicitly above as distributions on the interval  $[-1, 1]$ . For example the eigenfunctions  $b_j(z)$  in (3.11)

correspond to distributions,

$$(2j)!b_j(x) = \delta^{(2j)}(x-1) - \delta^{(2j)}(x+1) \quad (3.18)$$

(involving the  $2j$ th derivative of a delta function at each end point). By this we mean that applying  $\mathcal{F}$  to  $b_j(x)$  in (3.18) above gives the  $b_j(z)$  in (3.11). Similarly, for general  $\alpha$ ,

$$b_0(x) = e^{-i\alpha}\delta(x-1) - e^{i\alpha}\delta(x+1) \quad (3.19)$$

corresponds to (3.13). Magnetic field eigenfunctions taking this form of delta function distributions, located at the end points of the interval, have been discussed by Bayly (1992), Rado (1993) and Childress & Gilbert (1995), §9.5.2.

#### 4 Mainstream diffusion and eigenvalue corrections

The discussion of eigenfunctions without diffusion, of direct and adjoint operators, in the previous section is needed so that we can do perturbation theory to account for the introduction of diffusion. It is convenient to break up the interval  $[-1, 1]$  into a ‘mainstream’ part

$$-1 < x < 1, \quad x \text{ fixed as } \varepsilon \rightarrow 0, \quad (4.1)$$

and two boundary layers,

$$x \equiv -1 + \sqrt{\varepsilon}X \quad (\text{left}), \quad x \equiv 1 - \sqrt{\varepsilon}X \quad (\text{right}), \quad X \text{ fixed as } \varepsilon \rightarrow 0, \quad (4.2)$$

where the boundary conditions play an important role.

In this section we consider the mainstream region only, where we may approximate  $H_\varepsilon$  for any boundary condition by

$$G_\varepsilon c(x) \equiv G_\varepsilon^* c(x) = \int_{-\infty}^{\infty} G_\varepsilon(y) c(x+y) dy. \quad (4.3)$$

Our aim is to quantify the effects of diffusion in the mainstream region; in the next section we will consider the boundary layers that can occur. The attraction of mainstream diffusion is that it gives just a small perturbation of order  $\varepsilon$  to the eigenvalues of  $\mathcal{T}^*$  or  $\mathcal{T}$ , obtained for zero diffusion.

In fact one can discuss mainstream diffusion rigorously if we temporarily replace the symmetric Gaussian kernel (2.10), which has infinite support, by one which is symmetric, has unit area and has compact support, with  $g(x)$  only nonzero on  $[-\kappa, \kappa]$  for some  $\kappa > 0$ . In this case we can define an operator  $\mathcal{G}_\varepsilon^*$  on functions in  $\mathcal{B}^*$ , given by the same formula (4.3) for  $G_\varepsilon^*$ . Acting on a

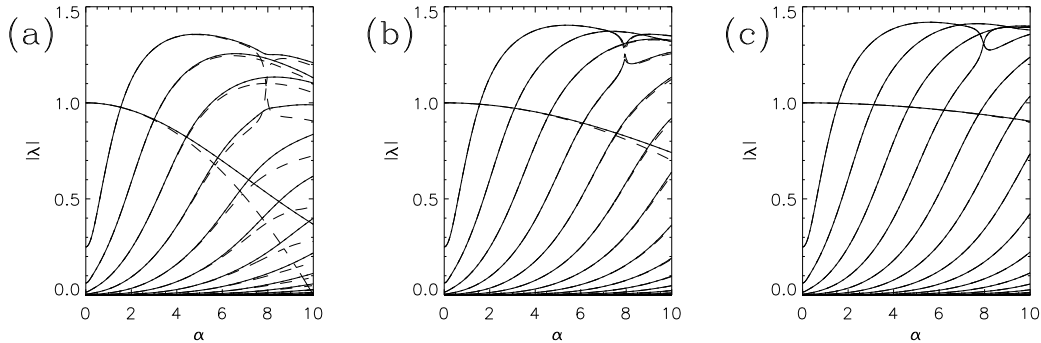


Fig. 11. Moduli of eigenvalues  $|\lambda|$  as a function of  $\alpha$  for the mainstream diffusive problem. The values for the diffusivity and resolution are (a)  $\varepsilon = 10^{-2}$ ,  $N = 128$ , (b)  $\varepsilon = 3 \times 10^{-3}$ ,  $N = 128$  and (c)  $\varepsilon = 10^{-3}$ ,  $N = 128$ . Dashed lines show eigenvalues computed by leading order perturbation theory (which overlap completely in (c)); see equation (4.10).

function  $c \in \mathcal{B}^*$ ,  $\mathcal{G}_\varepsilon^* c$  is only analytic in a smaller disc  $|z| < r - \kappa\sqrt{\varepsilon}$ . However  $\mathcal{T}^* \mathcal{G}_\varepsilon^* c$  is now analytic in  $|z| < 2(r - \kappa\sqrt{\varepsilon}) - 1$  and so is analyticity improving provided we take  $r > 1 + 2\kappa\sqrt{\varepsilon}$ .

Therefore, for a compactly supported kernel  $g(x)$ , the operator  $\mathcal{T}^* \mathcal{G}_\varepsilon^*$  is a compact operator and has a discrete spectrum of eigenvalues, shared with the adjoint operator  $\mathcal{G}_\varepsilon \mathcal{T}$ ; the latter operator will have eigenfunctions as hyperfunctions now supported on the interval  $[-1 - 2\kappa\sqrt{\varepsilon}, 1 + 2\kappa\sqrt{\varepsilon}]$ . Furthermore it may be established that, working in  $\mathcal{B}^*$

$$\|\mathcal{T}^*(\mathcal{G}_\varepsilon^* - \mathcal{I})\| \leq 2C e^{\alpha r/2} \varepsilon \kappa^2, \quad (C \equiv 8(r-1)^{-2}(r-1-2\kappa\sqrt{\varepsilon})^{-1}), \quad (4.4)$$

and so the eigenvalues of  $\mathcal{T}^* \mathcal{G}_\varepsilon^*$  converge to those of  $\mathcal{T}^*$  as  $\varepsilon \rightarrow 0$  (see Kato (1980), paper I).

To summarise, working in  $\mathcal{B}^*$ , diffusion in the mainstream can be thought of as diffusion on  $[-1, 1]$  with the boundary condition provided by analytically extending the function  $c$  on  $[-1, 1]$  beyond the endpoints and then applying a smoothing kernel. It gives small corrections, as is established rigorously for a compact smoothing kernel. Presumably the same is true for the full, non-compact Gaussian kernel (2.10) and we use this from now on as it is more convenient for computations; numerically, there is no difficulty in computing matrix elements for the operator  $\mathcal{G}_\varepsilon^*$  and these are given in appendix B. We have found eigenvalues of the combination  $\mathcal{T}^* \mathcal{G}_\varepsilon^*$  numerically for varying  $\varepsilon$ , and these are shown in figure 11, confirming the relatively harmless effect of mainstream diffusion.

We can compute the leading order correction by developing perturbation theory (which we will need also for the next section). Start with a normalised

eigenmode pair without diffusion,

$$\mathcal{T}b_0 = \lambda_0 b_0, \quad \mathcal{T}^*c_0 = \lambda_0 c_0, \quad \langle b_0, c_0 \rangle = 1. \quad (4.5)$$

We solve  $\mathcal{T}^*\mathcal{G}_\varepsilon^*c = \lambda c$  perturbatively by setting  $\varepsilon\mathcal{T}_1^* = \mathcal{T}^*(\mathcal{G}_\varepsilon^* - \mathcal{I})$  and expanding

$$\mathcal{T}^*\mathcal{G}_\varepsilon^* \equiv \mathcal{T}^* + \varepsilon\mathcal{T}_1^*, \quad c = c_0 + \varepsilon c_1 + \dots, \quad \lambda = \lambda_0 + \varepsilon\lambda_1 + \dots, \quad (4.6)$$

to obtain at order  $\varepsilon$

$$(\mathcal{T}^* - \lambda_0)c_1 = -\mathcal{T}_1^*c_0 + \lambda_1 c_0. \quad (4.7)$$

Then the solvability condition (integrating the left-hand side against the direct eigenmode  $b_0$ ) gives the leading order shift in eigenvalue as

$$\varepsilon\lambda_1^{\text{ms}} = \varepsilon\langle b_0, \mathcal{T}_1^*c_0 \rangle = \lambda_0\langle b_0, (\mathcal{G}_\varepsilon - \mathcal{I})c_0 \rangle, \quad (4.8)$$

where we have incorporated a label ‘ms’ to indicate that this is only the correction from mainstream diffusion. Note that weak diffusion for unit time on a smooth function can be expanded as

$$\mathcal{G}_\varepsilon^* = 1 + \varepsilon\partial_x^2 + \frac{1}{2}\varepsilon^2\partial_x^4 + \dots \quad (4.9)$$

and so the leading order eigenvalue shift can be rewritten to this order as

$$\delta\lambda^{\text{ms}} \equiv \varepsilon\lambda_1^{\text{ms}} \simeq \varepsilon\lambda_0\langle b_0, \partial_x^2 c_0 \rangle = \varepsilon\lambda_0 \sum_{n=0}^{\infty} \beta_n(n+1)(n+2)\gamma_{n+2} \quad (4.10)$$

where we have expanded  $b_0$  and  $c_0$  as in (3.9) and used (3.10).

For the exact eigenfunction (3.3) this shift is simply

$$\varepsilon\lambda_1^{\text{ms}} = -\varepsilon\alpha^2 e^{i\alpha}, \quad (4.11)$$

and for the eigenfunctions (3.2) at  $\alpha = 0$  the shift is zero using, say, (3.12). Figure 11 shows the leading order corrections as dashed lines; the agreement is good.

We can in fact calculate the exact analogues of the  $\alpha = 0$  eigenfunctions (3.2) for mainstream diffusion, satisfying  $\mathcal{T}^*\mathcal{G}_\varepsilon^*c = \lambda c$ , without perturbation theory.  $c_0$  is unchanged,

$$c_1(x) = x^3 - 3x^2 - (1 + 8\varepsilon)x + (3 + 8\varepsilon), \quad \lambda = \frac{1}{4}, \quad (4.12)$$

and  $c_n(x)$  is a polynomial of degree  $2n + 1$  in  $x$  and degree  $n$  in  $\varepsilon$ . Correspondingly,

$$b_j(x) = \frac{d^{2j}}{dx^{2j}} [e^{-(x-1)^2 3/16\varepsilon} - e^{-(x+1)^2 3/16\varepsilon}], \quad \lambda = 2^{-2j}. \quad (4.13)$$

These satisfy  $G_\varepsilon T b = \lambda b$ , where we now define  $T$  by (2.2). Relations similar to (3.12) continue to hold. The exact solution (3.3) remains an eigenfunction with mainstream diffusion, but now  $\lambda = e^{i\alpha - \varepsilon\alpha^2}$ .

With mainstream diffusion, the delta function distributions become spread out into Gaussians (4.13) localised near the endpoints  $x = \pm 1$  but spilling over them. In general we expect the effect of mainstream diffusion to have a similar smoothing effect on any distributional eigenfunction of  $\mathcal{T}$ . Note that the eigenfunctions (4.13) when re-expressed as hyperfunctions using (3.16) (and the integration extended to the whole real line), are singular all along the real axis, although the singularity becomes extremely weak as  $x \rightarrow \pm\infty$ , whereas for a compactly supported heat kernel this would not be the case. Thus for a Gaussian heat kernel a contour integral such as that in (3.6) becomes of questionable interpretation. On the other hand we can still compute numerically a sum as in (3.10), and this is how we proceed in our present pragmatic approach.

## 5 Boundary layers and scaling laws

We now consider the effect on growth rates of boundary layers, by considering the operators  $T_\varepsilon = H_\varepsilon T$  and  $T_\varepsilon^* = T^* H_\varepsilon^*$ . The problem is that unlike mainstream diffusion, the effect of boundary layers at the end points need not be a small perturbation. To see this consider a field  $c \in \mathcal{B}^* \subset L^2$ , so analytic in the disc  $\mathcal{D}$ ; plainly applying  $H_\varepsilon^*$  to it will yield an entire function, as it involves taking the values of  $c$  in  $[-1, 1]$ , extending them periodically and then diffusing. So  $H_\varepsilon^*$  can be considered as an operator, say  $\mathcal{H}_\varepsilon^*$  given by (2.6) and mapping  $\mathcal{B}^*$  to itself (in fact to entire functions). However if we then define  $\mathcal{T}_\varepsilon^* = T^* \mathcal{H}_\varepsilon^*$ , this need not be close to  $T^*$  as an operator in  $\mathcal{B}^*$ . The reason is that boundary layers generated by  $H_\varepsilon^*$  will depend as  $\exp(-(z \pm 1)^2/\varepsilon)$  near the endpoints  $z \simeq \pm 1$ , and this means that they will grow exponentially out into the complex plane, and ever more rapidly as  $\varepsilon \rightarrow 0$ . A norm such as (3.1) in  $\mathcal{B}^*$  is sensitive to this.

There is thus no reason *a priori* why the eigenvalues of  $\mathcal{T}_\varepsilon^*$  should be close to those of  $T^*$ ; however in some circumstances they may be. To find out when this may occur we adopt a pragmatic approach using perturbation theory. We start with an eigenmode pair (4.5) and write

$$\mathcal{T}_\varepsilon^* = T^* + \mathcal{T}_1^* + \mathcal{T}_2^* \quad (5.1)$$

with

$$\mathcal{T}_1^* = \mathcal{T}^*(\mathcal{G}_\varepsilon^* - \mathcal{I}), \quad \mathcal{T}_2^* = \mathcal{T}^*(\mathcal{H}_\varepsilon^* - \mathcal{G}_\varepsilon^*). \quad (5.2)$$

Here  $\mathcal{T}_1^*$  gives the mainstream diffusion correction  $\delta\lambda^{\text{ms}}$ , which has already been dealt with, and  $\mathcal{T}_2^*$  the boundary layer correction  $\delta\lambda^{\text{bl}}$ ; we do not scale explicitly by  $\varepsilon$  in what follows.

We first proceed with a naive, but very informative argument. Given an eigenfunction pair (4.5), to assess the shift in the eigenvalue from the effect of  $\mathcal{T}_2^*$  we should consider

$$\delta\lambda^{\text{bl}}(\varepsilon) = \langle b_0, \mathcal{T}_2^* c_0 \rangle, \quad (5.3)$$

by analogy with (4.8).

Now  $b_0$  is supported on  $[-1, 1]$ , and so we are only interested in the behaviour of  $\mathcal{T}_2^* c_0$  there. To calculate  $\mathcal{T}_2^* c_0$  consider first  $(\mathcal{H}_\varepsilon^* - \mathcal{G}_\varepsilon^*)c_0$  which has two boundary layers, one at each end point,

$$(\mathcal{H}_\varepsilon^* - \mathcal{G}_\varepsilon^*)c_0(1 - X\sqrt{\varepsilon}) = -2 \sum_{n \text{ even/odd}} \frac{c_0^{(n)}(1)}{n!} \varepsilon^{n/2} g_n(X), \quad (5.4a)$$

$$(\mathcal{H}_\varepsilon^* - \mathcal{G}_\varepsilon^*)c_0(-1 + X\sqrt{\varepsilon}) = -2 \sum_{n \text{ even/odd}} \frac{c_0^{(n)}(-1)}{n!} \varepsilon^{n/2} (-1)^n g_n(X), \quad (5.4b)$$

with  $n \geq 0$  even or odd for (I) or (C) respectively, and in the periodic case

$$(\mathcal{H}_\varepsilon^* - \mathcal{G}_\varepsilon^*)c(1 - X\sqrt{\varepsilon}) = - \sum_n \frac{c^{(n)}(1) - c^{(n)}(-1)}{n!} \varepsilon^{n/2} g_n(X), \quad (5.5a)$$

$$(\mathcal{H}_\varepsilon^* - \mathcal{G}_\varepsilon^*)c(-1 + X\sqrt{\varepsilon}) = \sum_n \frac{c^{(n)}(1) - c^{(n)}(-1)}{n!} \varepsilon^{n/2} (-1)^n g_n(X). \quad (5.5b)$$

Here for each boundary layer it is only necessary to retain two terms in the sums (2.7) and (2.8), and we have defined

$$g_n(s) = \int_0^\infty g(s+t)t^n dt \quad (5.6)$$

with

$$g_0(s) = \frac{1}{2} \operatorname{erfc}(s/2), \quad (5.7)$$

$$g_1(s) = -s g_0(s) + 2g(s), \quad (5.8)$$

$$g_2(s) = (s^2 + 2)g_0(s) - 2s g(s). \quad (5.9)$$

The boundary layers at each end are triggered by the action of diffusion: if the function  $c_0$  is periodically extended to fit the boundary condition (see (2.3)–(2.5)), a discontinuity in the  $n$ th derivative in this periodic extension generates the terms above.

Now when we apply  $\mathcal{T}^*$  to (5.4) or (5.5) the effect is to fold over the two boundary layers, with phase shifts, giving one boundary layer in  $\mathcal{T}_\varepsilon^* c_0$  at the left hand end, this function being zero in the mainstream and at the right-hand end. This has the form of a boundary layer of scale  $\sqrt{\varepsilon}$  and of magnitude  $\varepsilon^{n/2}$  where

$$n = 0 \quad (\text{insulating (I) for exact mode (3.3) only}), \quad (5.10a)$$

$$n = 0 \quad (\text{periodic (P) for exact mode (3.3) only}), \quad (5.10b)$$

$$n = 1 \quad (\text{conducting (C) for all modes}), \quad (5.10c)$$

$$n = 1 \quad (\text{periodic (P) for all other modes}), \quad (5.10d)$$

$$n = 2 \quad (\text{insulating (I) for all other modes}). \quad (5.10e)$$

The value of  $n$  gives the leading term in (5.4) or (5.5) for the perfect mode, and corresponds to a discontinuity in the  $n$ th derivative of  $c_0$  when the mode is periodically extended. Thus for the conducting case (C), any extended perfect mode  $c_0$  has a discontinuity of slope at the end points, corresponding to  $n = 1$ . For (I) and (P) boundary conditions, the situation depends on the mode in question, and the information in (3.4) and (3.5) becomes relevant. For the exact mode (except at  $\alpha = n\pi/2$ ), there is a discontinuity in value when extended with either boundary condition, giving  $n = 0$ . However the other modes are zero at both end points: for the (P) boundary condition there is a discontinuity in slope,  $n = 1$ , but for the (I) boundary condition there is only a discontinuity in second derivative,  $n = 2$ .

It is not worth writing out  $\mathcal{T}_2^* c_0$  in every case but, as an example we shall use later, for the (C) boundary condition and the exact mode (3.3) we obtain at leading order

$$\mathcal{T}_2^* c_0(-1 + \sqrt{\varepsilon}X) = \sqrt{\varepsilon}K_1 g_1(X/2) \quad (5.11)$$

with

$$K_1 = 2(e^{i\alpha}c'_0(-1) + e^{-i\alpha}c'_0(1)) = 2i\alpha(e^{3i\alpha} + 3e^{-i\alpha}). \quad (5.12)$$

It is not clear how to evaluate (5.3) in general, but we can easily obtain useful scaling information. If the diffusivity  $\varepsilon$  is multiplied by four, then the boundary layer thickness is doubled and the boundary layer strength multiplied by  $2^n$ . However also applying  $\mathcal{T}^*$  has the effect of pulling out the boundary layer and multiplying by a factor  $e^{i\alpha}$  locally. Using  $\mathcal{T}b_0 = \lambda_0 b_0$  we obtain the key scaling result

$$\delta\lambda^{\text{bl}}(\varepsilon) = \langle b_0, \mathcal{T}_2^* c_0 \rangle = \lambda_0^{-1} \langle \mathcal{T}b_0, \mathcal{T}_2^* c_0 \rangle = \lambda_0^{-1} \langle b_0, \mathcal{T}^* \mathcal{T}_2^* c_0 \rangle = \lambda_0^{-1} 2^{-n} e^{i\alpha} \delta\lambda^{\text{bl}}(4\varepsilon). \quad (5.13)$$

Assuming an exponential scaling law we obtain

$$\delta\lambda^{\text{bl}}(\varepsilon) = C\varepsilon^q, \quad 2q = n + (\log \lambda_0 - i\alpha)/\log 2. \quad (5.14)$$

Strictly there could be oscillations of period  $\log 4$  in  $\log \varepsilon$  superposed, but we

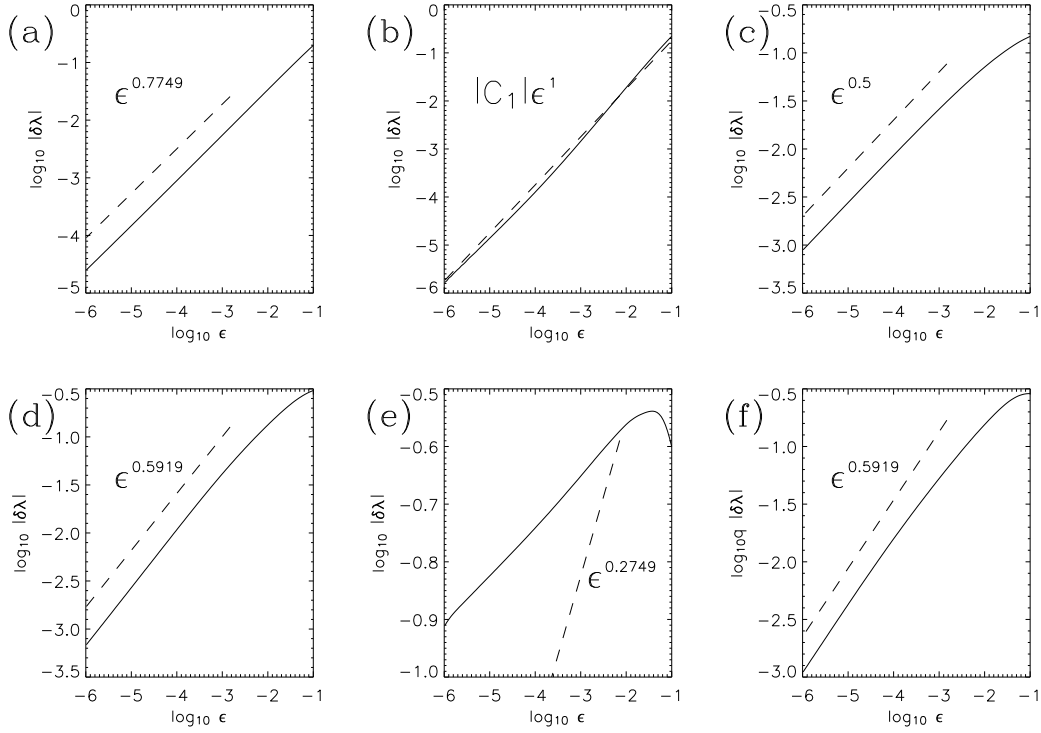


Fig. 12. Comparison of scaling laws:  $\log_{10} |\lambda(\varepsilon) - \lambda_0|$  (solid) and a power law (dashed) are plotted against  $\log_{10} \varepsilon$  for the leading, most unstable branch. In (a)  $\alpha = 1$  (I), power law  $\varepsilon^{0.7749}$ , (b)  $\alpha = 2$  (I), power law  $|C_1|\varepsilon^1$ , (c)  $\alpha = 1$  (C), power law  $\varepsilon^{0.5}$ , (d)  $\alpha = 2$  (C), power law  $\varepsilon^{0.5919}$ , (e)  $\alpha = 1$  (P), power law  $\varepsilon^{0.2749}$  and (f)  $\alpha = 2$  (P), power law  $\varepsilon^{0.5919}$ .

will ignore this subtle feature; it can sometimes be just about observed in the passive scalar problem in paper III.

This gives some important information. First, for perturbation theory to be self-consistent, we require the correction  $\delta\lambda^{\text{bl}}$  to be small, scaling to zero as  $\varepsilon \rightarrow 0$ . This requires  $\text{Re } q > 0$ , and so  $|\lambda_0| > 2^{-n}$ . If this condition is satisfied, diffusion will be a small perturbation to the perfect mode and it will be robust; if it fails to be satisfied, there is no reason why diffusion should not destroy the mode — it is likely to be delicate. For all perfect modes other than the exact mode, combining this information with (5.10) gives immediately the criteria (2.18), (2.20) and (2.22) for modes to be robust under each boundary condition. For the exact mode itself,  $|\lambda| = 1$  and so the mode is robust to the (C) boundary condition,  $n = 1$ , but is delicate for (I) or (P) boundary conditions,  $n = 0$ , in agreement with results in section 2.

The other information given is the way in which  $\lambda(\varepsilon)$  approaches  $\lambda_0$  for a robust mode: for the boundary layer correction this is as a complex power  $q$  of  $\varepsilon$  in (5.14), so as a real power law with oscillations in real and imaginary parts superposed. The mainstream correction is of order  $\varepsilon$ , given explicitly by (4.10).

To test our results figure 12 shows results for a number of different cases; in each case the  $|\lambda(\varepsilon) - \lambda_0|$  (solid) is plotted, together with the theoretical power law (dashed), against  $\varepsilon$  on a log–log scale.

In (a) the insulating boundary condition is used for  $\alpha = 1$ ; the mode decays,  $|\lambda_0| < 1$ , and there is good agreement between the actual correction and the predicted power law with  $\text{Re } q \simeq 0.7749$ . In (b) the (I) boundary condition is again used, but now for the growing mode with  $\alpha = 2$ . Here the predicted boundary layer correction scales as  $\varepsilon^{1.0919}$ , which is (just) steeper than the mainstream correction, which may be computed as  $C_1\varepsilon$  with  $C_1 \simeq -0.62546 - 1.6751i$  obtained by computing  $c_0$  and  $b_0$  in (3.9) for this mode numerically and then using (4.10). The comparison between the numerical results and this mainstream correction is good.

The remaining parts (c–f) of figure 12 show results for (C) and (P) boundary conditions. The comparison is excellent except for (e) when the numerical correction falls off much more slowly than the prediction, for (P) and  $\alpha = 1$ . This appears to occur because of the interaction between two modes, a possibility not included within our theory. Looking back at figure 4 we see that at  $\alpha = 1$  the non-diffusive mode (seen as a perfect mode in figure 9 for zero diffusion) is extremely close to the 3-peaked diffusive branch that appears for the (P) boundary condition. We confirm this behaviour of the diffusive branch towards the end of the next section. The slow convergence seen is likely to be the reason for the diffusive dynamo action for  $\alpha < \pi/2$  reported in Childress & Gilbert (1995) (figure 9.5); in our simulations we do not see evidence of dynamo action for  $\alpha < \pi/2$  in the limit  $\varepsilon \rightarrow 0$ .

Note that the corrections in figure 12(b,d,f) are for the same underlying robust perfect mode. Those in figure 12(a,e) are also for the same perfect mode, but (c) refers to the exact mode, which is only robust for the (C) boundary condition.

Our perturbation theory for the boundary layer correction appears to work well in giving the correct scaling results, but is actually quantitatively incorrect, as the leading order boundary layer correction is not given by (5.3)! The problem is that if one imagines developing perturbation theory to higher orders, the next correction will arise from applying  $\mathcal{H}_\varepsilon^*$  to the boundary layer we have obtained above, e.g., in (5.11), and because the layer has a spatial scale of order  $\sqrt{\varepsilon}$  the correction will be of a similar magnitude  $O(\varepsilon^{n/2})$  to the original boundary layer, and will give a correction of the same order as (5.3).

What this indicates is that the proper procedure is to solve an integral equation for the structure of the boundary layer, forced by the term  $\mathcal{T}_2^*c_0$ , in which diffusion enters in a non-perturbative fashion. Only then should one integrate against  $b_0$  as in (5.3) to obtain the eigenvalue correction. Having given all these

caveats, of course the scaling result (5.3) will continue to hold in this more careful approach, as it depends only on the spatial scale and magnitude of the boundary layer, and the scaling property of the distributional eigenfunction  $b_0$ .

There is no problem in writing down the integral equation for the boundary layer structure in a given case and solving it numerically. The problem arises in employing a solvability condition, since this involves integrating this boundary layer, known numerically for  $x = -1 + \sqrt{\varepsilon}X$  and  $X = O(1)$ , against  $b_0$ , which is generally only known as a power series of the form (3.9). It is not clear how to do this integration robustly, and we will therefore not pursue this further in general. It can be done for the passive scalar problem since more explicit formulae are known, and we refer the reader to paper III for further information. Suffice it to say that this paper confirms that the scaling arguments presented here remain valid when backed up by more detailed analysis.

## 6 Boundary layer theory for the exact branch

One case where the boundary layer eigenvalue correction can be calculated without too much difficulty is for the exact branch (3.3) with the (C) boundary condition (figure 3), which we study in this section, together with a boundary layer problem that gives the diffusive 3-peaked branch seen in figure 4.

For the diffusive correction to the exact mode, we need to solve

$$\mathcal{T}_\varepsilon^* c = (\mathcal{T}^* + \mathcal{T}_1^* + \mathcal{T}_2^*)c = \lambda c \quad (6.1)$$

approximately (see (5.2)). We expand

$$c = c_0 + c_1 + \dots, \quad \lambda = \lambda_0 + \lambda_1 + \dots, \quad (6.2)$$

where  $c_0$  and  $\lambda_0$  give the exact mode (3.3) satisfying  $\mathcal{T}^* c_0 = \lambda_0 c_0$ . The quantities  $c_1$  and  $\lambda_1 \equiv \delta\lambda^{\text{bl}}$  give the leading corrections, and are of order  $\sqrt{\varepsilon}$ .

We substitute this expansion into (6.1), subtract  $\mathcal{T}^* c_0 = \lambda_0 c_0$  and retain all possible leading terms (which will be of order  $\sqrt{\varepsilon}$ ) to give

$$\mathcal{T}_2^* c_0 + \mathcal{T}_\varepsilon^* c_1 = \lambda_0 c_1 + \lambda_1 c_0. \quad (6.3)$$

Here we have neglected  $\mathcal{T}_1^* c_0$ , mainstream diffusion, giving an  $O(\varepsilon)$  correction already discussed in the previous section. The leading correction  $c_1$  will vary on the  $X$ -scale within the boundary layer, but on the larger  $x$ -scale in the mainstream.

We now focus on the left-hand boundary layer itself, taking  $X = O(1)$ ,  $x \simeq -1$ ; there is no right hand boundary layer. We have evaluated  $\mathcal{T}_2^* c_0$  for this case already in (5.11) and (5.12) above. Also in the boundary layer we have

$$\mathcal{T}_\varepsilon^* c_1(-1 + \sqrt{\varepsilon}X) \simeq e^{i\alpha} \int_0^\infty [g(X/2 + Y) + g(X/2 - Y)] c_1(-1 + \sqrt{\varepsilon}Y) - e^{-i\alpha} c_1(1), \quad (6.4)$$

approximating the shear to leading order, and neglecting diffusion near  $x = 1$  (where it would give an order  $\varepsilon$  correction). Also  $c_1(1) = 0$  since  $c(1) = 0$  may be deduced from  $\mathcal{T}_\varepsilon^* c = \lambda c$ .

Now put

$$c_1(-1 + \sqrt{\varepsilon}X) = \sqrt{\varepsilon} e^{-i\alpha} K_1 d(X) \quad (6.5)$$

to give from (6.3) the integral equation

$$g_1(X/2) + \int_0^\infty [g(X/2 - Y) + g(X/2 + Y)] d(Y) dY = d(X) + K, \quad (6.6)$$

with  $K$  defined by

$$K = \lambda_1 c_0(-1) / \sqrt{\varepsilon} K_1. \quad (6.7)$$

This integral equation is degenerate in that a constant may be added to a solution  $d(X)$  to obtain another solution. With this there is a solvability condition, in that a solution only exists for a certain value of  $K$ . This may be found numerically by setting  $K$  and then attempting to obtain  $d(X)$  by straightforward iteration of the left-hand side of (6.6). It is found numerically that

$$K \simeq 0.3257355 \quad (6.8)$$

and this fixes the correction to the growth rate as

$$\lambda_1 = \sqrt{\varepsilon} K K_1 / c_0(-1) = -\alpha K \sqrt{\varepsilon} \frac{e^{3i\alpha} + 3e^{-i\alpha}}{\sin 2\alpha}. \quad (6.9)$$

Note that taking the limit  $\alpha \rightarrow 0$  gives the result (2.21) with the constant  $K$  pinned down conclusively.

The structure of the boundary layer obtained for this value of  $K$  is shown in figure 13 and it has a logarithmic tail of the form

$$d(X) \simeq -K \log X / \log 2 + C_2 \quad (X \rightarrow \infty). \quad (6.10)$$

The constant  $C_2$  would be fixed by matching to a mainstream solution of  $\mathcal{T}_\varepsilon^* c_1 \simeq \mathcal{T}^* c_1 = \lambda_0 c_1 + \lambda_1 c_0$ , but we do not need to do this.

To confirm this theory figure 14 shows the moduli of the eigenvalues  $|\lambda|$  obtained numerically for the exact mode and the (C) boundary condition (solid), while the approximation  $|\lambda_0 + \lambda_1|$  is shown dashed. The agreement is excellent

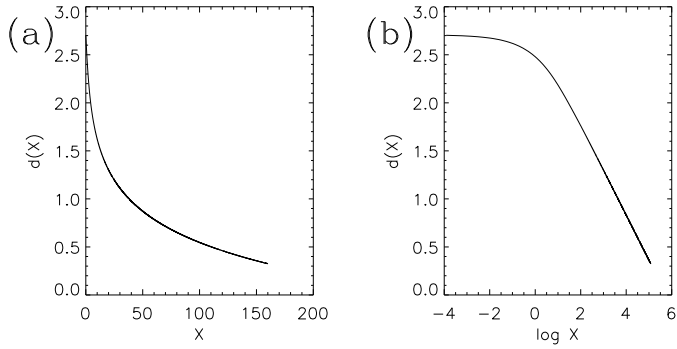


Fig. 13. Structure of the boundary layer. In (a)  $d(X)$  is plotted against  $X$ , and in (b) against  $\log X$ .

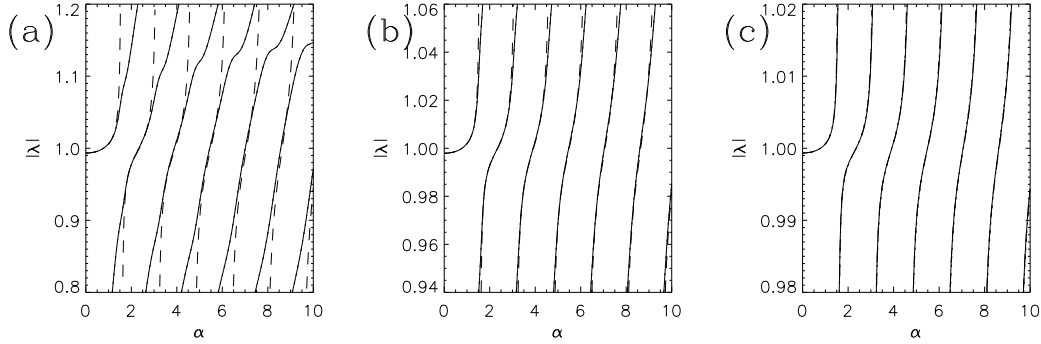


Fig. 14. Moduli of eigenvalues  $|\lambda|$  for the exact mode against  $\alpha$ . Numerical results for the (C) boundary condition are shown solid. Dashed lines show the asymptotic approximation  $|\lambda_0 + \lambda_1|$ ; see (3.3) and (6.9). In (a)  $\varepsilon = 10^{-4}$ ,  $N = 512$ , (b)  $\varepsilon = 10^{-5}$ ,  $N = 1024$  and (c)  $\varepsilon = 10^{-6}$ ,  $N = 1024$ .

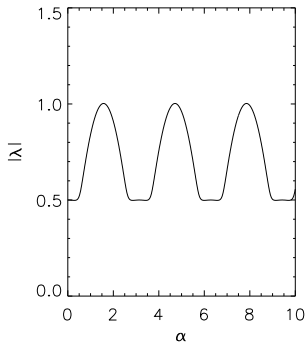


Fig. 15. Eigenvalues  $|\lambda|$  as a function of  $\alpha$  for the unforced periodic boundary layer problem (6.12).

as  $\varepsilon$  is reduced from (a) to (c), with the extent of the vertical scale changing in concert.

Finally we consider the diffusive 3-peaked mode seen in figure 4. This has no perfect counterpart, and so it is probable that this mode is driven from the boundary layer rather than forced by a mainstream perfect mode. We consider

a mode with  $\mathcal{T}_\varepsilon^*c = \lambda c$ , and put

$$c(-1 + \sqrt{\varepsilon}X) = d(X). \quad (6.11)$$

Noting that  $c(1) = 0$  by virtue of  $\mathcal{T}_\varepsilon^*c = \lambda c$ , we may obtain the integral equation

$$\int_0^\infty [e^{i\alpha}g(X/2 - Y) - e^{-i\alpha}g(X/2 + Y)]d(Y) dY = \lambda d(X). \quad (6.12)$$

Here we have again assumed that  $c$  varies on the rapid,  $X$ -scale in the boundary layer, and on the  $x$ -scale outside.

For a given value of  $\alpha$  this equation may be iterated to obtain a free decay rate  $\lambda$  and these are shown in figure 15 as a function of  $\alpha$ . Comparison with figure 4 indicates that clearly this is the origin of the diffusive mode seen; this boundary layer solution would be matched onto a (forced) mainstream part, but we need not determine this. Note the exact solutions: for  $\alpha = n\pi$ ,  $\lambda = \frac{1}{2}e^{i\alpha}$ , and  $d(X) = X$ , while for  $\alpha = (n + \frac{1}{2})\pi$ ,  $\lambda = e^{i\alpha}$ , and  $d(X) = 1$ . This latter case has an eigenvalue coinciding with the exact mode (3.3), which explains the slow convergence seen in figure 12(e).

## 7 Discussion

We have studied dynamo action in the SFS map by means of numerical simulation and then asymptotic approximations using a combination of boundary layer theory and the diffusionless framework developed in paper I. We have been able to show how diffusion can destroy perfect eigenmode branches, and that this depends on the structure of the branch, its growth rate, and the boundary conditions, as found by Bayly & Childress (1988) and Finn & Ott (1990). However we have found that all perfect branches where the modes are growing, with  $|\lambda| > 1$ , are unaffected by diffusion, regardless of their structure, or the boundary conditions. Thus our study gives support for fast dynamo action in the SFS map for all boundary conditions.

We should note that diffusion is a strong effect in the SFS map, because of its discontinuous nature, and essentially there is a competition between the growth of the field through stretching, in the mainstream interior, and its destruction through diffusion. For  $T^*$  this destruction occurs in the boundary layer at the left end point (which is continually being stretched into the interior) or for  $T$  by the accumulation of boundary layers in the interior. Essentially if the perfect mode grows fast enough (at least  $|\lambda| > 1$ ), the stretching wins. This paper has proceeded by asymptotic approximation, and while it has captured key aspects of the SFS model, this does not constitute a proof.

The key problem is to show that eigenvalues  $\mathcal{T}^*$  with  $|\lambda|$  large enough are only perturbed when one introduces diffusion giving  $\mathcal{T}_\varepsilon^*$ . This is not obvious because only some eigenvalues are perturbed, others disappear completely.

In terms of interpreting our results for the limit of weak diffusion it is worth reintroducing the parameter  $k$  which was set to  $k = 1$  after (2.1). In the body of this paper we have discussed growth rates  $\lambda(\alpha, \varepsilon)$ . For a general  $k$ , the parameter  $\alpha$  becomes  $\alpha k$  once again and there is in addition an exponential damping factor  $\exp(-\varepsilon k^2)$ , which we ignored. The growth in a given mode per iteration of  $T_\varepsilon$  will be by a factor of  $\lambda(\alpha k, \varepsilon)e^{-\varepsilon k^2}$ . If we now consider a given fluid flow, modelled by the SFS map with a given value of  $\alpha$ , then roughly speaking the range of modes  $\pi/2\alpha < k \leq O(\varepsilon^{-1/2})$  will be destabilised, and this range will increase as  $\varepsilon$  is reduced. These modes will be competing for the optimal growth rate, and since we know little about the structure of the peaks in  $|\lambda|$  in figure 9 over a wide range of  $\alpha$ , it is unclear which modes will be dominant for small  $\varepsilon$ . This suggests that the structure of a growing field in the  $z$ -direction could be quite complicated, at small  $\varepsilon$ .

The theory we have developed has exploited the fact that for  $T$  there is contraction of structure in the  $x$ -direction, while for  $T^*$  the structure is expanded in this direction, the  $y$ -direction being trivial in both cases. It would be interesting to attempt to extend the above theory to hyperbolic dynamo systems with two non-trivial directions, one stretching and one contracting, for example, cat maps with shear (Aurell & Gilbert, 1993). In this case  $T$  and  $T^*$  are on an equal footing as neither gives a simpler system. However it should still be possible to define  $\mathcal{T}$  and  $\mathcal{T}^*$  and seek eigenfunctions, following ideas of Rugh (1992). The procedure would be to divide space into a Markov partition, and in each piece to expand eigenfunctions in powers of a coordinate  $z_1$  in the expanding direction and in inverse powers of a coordinate  $z_2$  in the contracting direction. This would give perfect modes with eigenvalues that could be compared with eigenfunctions in  $L^2$  for an operator  $T_\varepsilon$  that incorporates diffusion.

Finally note that the dynamo systems discussed here are based on underlying hyperbolic maps, and this is crucial in getting the machinery developed in this series of papers to work; the challenge of studying non-hyperbolic maps remains considerable.

## A Appendix: matrix elements in $L^2$

Here we list bases and matrix elements used for numerical computations of eigenvalues and eigenvectors for magnetic fields with  $\varepsilon > 0$ , lying in  $L^2$ . The

basis for the insulating (I) boundary condition is indexed by  $n \geq 1$ ,

$$\psi_n(x) = \sin \frac{1}{2}n\pi(x+1) \quad (n \geq 1) \quad (\text{I}). \quad (\text{A.1})$$

For the conducting (C) boundary condition we use, indexed by  $n \geq 0$ ,

$$\psi_n(x) = \cos \frac{1}{2}n\pi(x+1) \quad (n \geq 1), \quad \psi_0(x) = 2^{-1/2} \quad (\text{C}), \quad (\text{A.2})$$

and for the periodic (P) boundary condition we use, indexed by  $n \geq 0$ ,

$$\psi_n(x) = \begin{cases} 2^{-1/2} & (n = 0), \\ \cos q\pi x & (n \text{ even}, n = 2q > 0), \\ \sin q\pi x & (n \text{ odd}, n = 2q - 1). \end{cases} \quad (\text{P}), \quad (\text{A.3})$$

Define  $F(k) = 2k^{-1} \sin k$  and coefficients  $\nu_m$  by

$$\nu_0 = 2^{-1/2}, \quad \nu_m = 1 \quad (m > 0). \quad (\text{A.4})$$

The matrix elements for (I) (upper sign) and (C) (lower sign) with the appropriate legal values for  $m$  and  $n$  are,

$$\begin{aligned} T_{mn} = \mp \frac{1}{4} \nu_m \nu_n [ & (e^{i(\frac{\alpha}{2} - \frac{m\pi}{4} - \frac{n\pi}{2})} \pm e^{i(-\frac{\alpha}{2} - \frac{3m\pi}{4} + \frac{n\pi}{2})}) F(\frac{\alpha}{2} + \frac{m\pi}{4} + \frac{n\pi}{2}) \\ & + (\mp e^{i(\frac{\alpha}{2} - \frac{m\pi}{4} + \frac{n\pi}{2})} - e^{i(-\frac{\alpha}{2} - \frac{3m\pi}{4} - \frac{n\pi}{2})}) F(\frac{\alpha}{2} + \frac{m\pi}{4} - \frac{n\pi}{2}) \\ & + (\mp e^{i(\frac{\alpha}{2} + \frac{m\pi}{4} - \frac{n\pi}{2})} - e^{i(-\frac{\alpha}{2} + \frac{3m\pi}{4} + \frac{n\pi}{2})}) F(\frac{\alpha}{2} - \frac{m\pi}{4} + \frac{n\pi}{2}) \\ & + (e^{i(\frac{\alpha}{2} + \frac{m\pi}{4} + \frac{n\pi}{2})} \pm e^{i(-\frac{\alpha}{2} + \frac{3m\pi}{4} - \frac{n\pi}{2})}) F(\frac{\alpha}{2} - \frac{m\pi}{4} - \frac{n\pi}{2}) ]. \end{aligned} \quad (\text{A.5})$$

For the heat kernel  $H_\varepsilon$  we have for either of these bases,

$$H_{\varepsilon mn} = e^{-\varepsilon n^2 \pi^2 / 4} \delta_{mn}. \quad (\text{A.6})$$

For the (P) boundary condition,

$$\begin{aligned} T_{mn} = \frac{1}{4} \nu_m \nu_n i^{\frac{1}{2}(\rho-1)} i^{\frac{1}{2}(\sigma-1)} \\ \times [\rho (\sigma e^{i\frac{1}{2}(\alpha+p\pi)} - e^{i\frac{1}{2}(-\alpha-p\pi)}) (F(\frac{\alpha}{2} + \frac{p\pi}{2} + q\pi) + \sigma F(\frac{\alpha}{2} + \frac{p\pi}{2} - q\pi)) \\ + (\sigma e^{i\frac{1}{2}(\alpha-p\pi)} - e^{i\frac{1}{2}(-\alpha+p\pi)}) (F(\frac{\alpha}{2} - \frac{p\pi}{2} + q\pi) + \sigma F(\frac{\alpha}{2} - \frac{p\pi}{2} - q\pi))], \end{aligned} \quad (\text{A.7})$$

where we let  $(p, \rho) = (m/2, 1)$  if  $m$  is even, and  $(\frac{1}{2}(m+1), -1)$  if  $m$  is odd. We define  $(q, \sigma)$  similarly in terms of  $n$ . For the heat kernel,

$$H_{\varepsilon mn} = e^{-\varepsilon p^2 \pi^2} \delta_{mn}. \quad (\text{A.8})$$

Note that to obtain numerically eigenvalues and eigenvectors, these infinite matrices are truncated to size  $m, n \leq N$ , replacing  $T_\varepsilon$  by an operator  $T_{\varepsilon N} \equiv$

$P_N T_\varepsilon$ , where  $P_N$  is a projection. We are guaranteed that the eigenvalues obtained numerically will converge as  $N \rightarrow \infty$  for any fixed  $\varepsilon > 0$ . For example for the (I) boundary condition and working in  $L^2$ ,

$$\|T_\varepsilon - T_{\varepsilon N}\| = \|(I - P_N)H_\varepsilon T\| \leq \|(I - P_N)H_\varepsilon\| \|T\| \leq 2e^{-\varepsilon(N+1)^2\pi^2/4} \rightarrow 0 \quad (\text{A.9})$$

in this limit (also see the discussion in §7.1 of paper I).

## B Appendix: matrix elements in $\mathcal{B}$

We now give matrix elements with respect to the bases (3.8) of  $\mathcal{B}$  and  $\mathcal{B}^*$ ,

$$\mathcal{T}_{mn}^* = \langle e_m, \mathcal{T}^* e_n^* \rangle. \quad (\text{B.1})$$

For the operator  $\mathcal{T}^*$  we have from paper I with  $i \rightarrow -i$ ,

$$\mathcal{T}_{mn}^* = r^{m-n} \sum_{p=\max(m-n,0)}^m \frac{2^{-n}(-1)^m n!}{p!(m-p)!(n-m+p)!} \left(\frac{-i\alpha}{2}\right)^p [e^{i\alpha/2}(-1)^{n+p} - e^{-i\alpha/2}]. \quad (\text{B.2})$$

Note that for  $\alpha = 0$  this matrix has  $\mathcal{T}_{mn}^* = 0$  for  $m > n$  and so is upper triangular, with entries 0, 1, 0,  $\frac{1}{4}$ , 0,  $\frac{1}{16}$ , etc., along the diagonal, giving the eigenvalues in (3.2). For matrix elements of  $\mathcal{G}_\varepsilon^*$  we have all elements zero except

$$\mathcal{G}_{\varepsilon mn}^* = \left(\frac{2\varepsilon}{r^2}\right)^{\frac{1}{2}(n-m)} \frac{n!}{m!(n-m)!} (n-m-1)(n-m-3)\cdots 5 \cdot 3 \cdot 1, \quad (\text{B.3})$$

$(n \geq m, n-m \text{ even}).$

Note that the matrix for  $\mathcal{G}_\varepsilon^*$  is upper triangular with elements unity along the diagonal. Although requiring that the constant  $r > 1$  is essential for the properties of the operators  $\mathcal{T}$  and  $\mathcal{T}^*$ , for numerical computations the specific value of  $r$  is unimportant, and  $r$  can be set to one.

## Acknowledgements

Much of this work developed out of collaboration with Steve Childress and Bruce Bayly, who together first realised the importance of discussing eigenfunctions taking the form of distributions, and the relevance of boundary layer theory. I am also grateful to Erik Aurell, Anton Deitmar, Ben Mestel and Jean-Luc Thiffeault for valuable discussions and references.

This series of studies was begun at the ‘Geometry and Topology of Fluid Flows’ programme held at the Isaac Newton Institute in Cambridge (Autumn

2000) and completed at the programme ‘Magnetohydrodynamics of Stellar Interiors’ (Autumn 2004). I am grateful to the organisers of both programmes and directors of the Institute for inviting me to participate.

## References

- Aurell, E. & Gilbert, A.D. “Fast dynamos and determinants of singular integral operators,” *Geophys. Astrophys. Fluid Dyn.* **73**, 5–32 (1993).
- Backus, G. “A class of self-sustaining dissipative spherical dynamos,” *Ann. Physics* **4**, 372–447 (1958).
- Balmforth, N.J., Cvitanović, P., Ierley, G.R., Spiegel, E.A. & Vattay, G. “Advection of vector fields by chaotic flows,” In: *Stochastic Processes in Astrophysics*, pp. 148–160. Annals New York Acad. Sci., vol. 706 (1993).
- Bayly, B.J. “Infinitely conducting dynamos and other horrible eigenproblems,” In: *Nonlinear Phenomena in Atmospheric and Oceanic Sciences* (Eds. Carnevale, G.F. and Pierrehumbert, R.T.), pp. 139–176, IMA Series in Mathematics and its Applications, vol. 40. Springer–Verlag (1992).
- Bayly, B.J. “Maps and dynamos,” In: *Lectures on Solar and planetary dynamos* (Eds. Proctor, M.R.E. and Gilbert, A.D.), pp. 305–329. Cambridge University Press (1994).
- Bayly, B.J. & Childress, S. “Construction of fast dynamos using unsteady flows and maps in three dimensions,” *Geophys. Astrophys. Fluid Dyn.* **44**, 211–240 (1988).
- Bayly, B.J. & Childress, S. “Unsteady dynamo effects at large magnetic Reynolds numbers,” *Geophys. Astrophys. Fluid Dyn.* **49**, 23–43 (1989).
- Bollobás, B. *Linear Analysis: An Introductory Course*, Cambridge University Press (1990).
- Childress, S. & Gilbert, A.D. *Stretch, Twist, Fold: The Fast Dynamo*, Springer–Verlag (1995).
- Finn, J.M. & Ott, E. “Chaotic flows and fast magnetic dynamos,” *Phys. Fluids* **31**, 2992–3011 (1988).
- Finn, J.M., Ott, E. “The fast kinematic magnetic dynamo and the dissipationless limit,” *Phys. Fluids B* **2**, 916–926 (1990).
- Galloway, D.J. & Proctor, M.R.E. “Numerical calculations of fast dynamos for smooth velocity fields with realistic diffusion,” *Nature* **356**, 691–693 (1992).
- Gilbert, A.D. “Advection fields in maps: I. Magnetic flux growth in the stretch–fold–shear map,” *Physica D* **166**, 167–196 (2002). (Referred to herein as paper I.)
- Gilbert, A.D. “Advection fields in maps: III. Passive scalar decay in baker’s maps,” In preparation (2004). (Referred to herein as paper III.)
- Kato, T. *Perturbation Theory for Linear Operators*, Springer–Verlag (1980).
- Klapper, I. “A study of fast dynamo action in chaotic helical cells,” *J. Fluid Mech.* **239**, 359–381 (1992).

- Mestel, B.D., Osbaldestin, A.H. & Winn, B. “Golden mean renormalization for the Harper equation: the strong coupling fixed point,” *J. Math. Phys.* **41**, 8304–8330 (2000).
- Otani, N.F. “A fast kinematic dynamo in two-dimensional time-dependent flows,” *J. Fluid Mech.* **253**, 327–340 (1993).
- Rado, A. *Onset and Intermittency in the SFS Map*, MS Thesis, Courant Institute of Mathematical Sciences, New York University (1993).
- Rugh, H.H. “The correlation spectrum for hyperbolic analytic maps” *Nonlinearity* **5**, 1237–1263 (1992).
- Schlichtkrull, H. *Hyperfunctions and Harmonic Analysis on Symmetric Spaces*. Birkhäuser (1984).
- Trefethen, L.M. “Pseudospectra of linear operators,” *SIAM Review* **39**, 383–406 (1997).